

# Analysis of kinetic freeze out temperature and transverse flow velocity in nucleus-nucleus and proton-proton collisions at same center of mass energy

M. Waqas<sup>1,\*</sup>, G. X. Peng<sup>1,2,3 †</sup>, Z. Wazir<sup>4, ‡</sup>,  
Hai-Ling Lao<sup>5, §</sup>

<sup>1</sup> School of Nuclear Science and Technology, University of Chinese Academy of Sciences, Beijing 100049, China

<sup>2</sup> Theoretical Physics Center for Science Facilities, Institute of High Energy Physics, Beijing 100049, China

<sup>3</sup> Synergetic Innovation Center for Quantum Effects & Application, Hunan Normal University, Changsha 410081, China,

<sup>4</sup> Department of physics, Ghazi university, Dera ghazi khan, Pakistan,

<sup>5</sup> Center for high energy physics, Peking university, Beijing 100871, China

**Abstract:** Transverse momentum spectra of **different types of** identified charged particles in central Gold-Gold (Au-Au) collisions, and inelastic (INEL) or non-single-diffractive (NSD) proton-proton (pp) collisions at the Relativistic Heavy Ion Collider (RHIC), as well as in central and peripheral Lead-Lead (Pb-Pb) collisions, and INEL or NSD pp collisions at the Large Hadron Collider (LHC) are analyzed by the blast wave model with Tsallis statistics. The model results are approximately in agreement with the experimental data measured by STAR, PHENIX and ALICE Collaborations in special transverse momentum ranges. Kinetic freeze out temperature and transverse flow velocity are extracted from the transverse momentum spectra of the particles. It is shown that kinetic freeze out temperature of the emission source depends on mass of the particles, which reveals the **mass differential kinetic freeze out scenario** in collisions at RHIC and LHC. Furthermore, the kinetic freeze out temperature and transverse flow velocity in central nucleus-nucleus (AA) collisions are larger than in peripheral collisions, and both of them are slightly larger in peripheral nucleus-nucleus collisions or almost equivalent to that in pp proton-proton collisions at the same center of mass energy which shows their similar thermodynamic nature.

**Keywords:** Kinetic freeze out temperature, transverse flow velocity, transverse momentum spectra, high energy collisions.

**PACS:** 25.75.Ag, 25.75.Dw, 24.10.Pa

## 1 Introduction

It is a common sense that transition to quark matter happens in special circumstances, e.g. astronomically at the core of a dense compact star [1,2], and territorially in relativistic heavy-ion collisions [3-5]. In later case, when the incident energy of nucleus is in the order of GeV, a hot matter called quark-gluon plasma (QGP) is produced. The QGP behaves like nearly a perfect fluid and it expands very rapidly and emit large amount of radiations which result in cooling of the matter. In fact, its direct detection and study is extremely difficult due to having a very short life time, but the particles or radiations emission from QGP are good objects to observe the QGP properties. One of the most

central concepts in thermodynamics and statistical mechanics [6] is the temperature, which is very important in both the thermal and subatomic physics, because it has extremely wide applications in experimental measurements and theoretical studies. Four types of different temperatures namely initial temperature ( $T_i$ ), chemical freeze out temperature ( $T_{ch}$ ), effective temperature ( $T_{eff}$ ) and kinetic freeze out temperature ( $T_0$ ) can be found in literature. The detailed explanation of these temperatures is given in one of our recent work [7].  $T_0$  describes the excitation degree of the interacting system at the stage of thermal/kinetic freeze out. A natural question arises that how many kinetic freeze out temperatures ( $T_0$ ) are there at the stage of thermal freeze out. In general, both  $T_0$  and  $T_{ch}$  happens simultane-

\*Corresponding author. Email (M. Waqas): waqas\_phy313@yahoo.com

†Corresponding author. Email (G. X. Peng): gxpeng@ucas.ac.cn

‡Z.Wazir: zafar\_wazir@yahoo.com

§H-L Lao: hailinglao@pku.edu.cn

ously or the former happens later. The behavior of  $T_{\text{ch}}$  is studied in [8, 9] while  $T_0$  has a more complex situation. There are three main issues to be checked. It is known that  $T_0$  **initially, increase sharply in central collisions from low energy ranges upto almost 10 GeV in Beam Energy Scan (BES) energies** [10, 11], and then saturates upto 39 GeV. However after 39 GeV, this tendency can be saturated, decrescent or incresecent. It is needed to check the correct tendency. Secondly,  $T_0$  can be slightly larger in central collision, or slightly smaller than or approximately equal to that in peripheral collision. It is needed to check that which collisions has larger  $T_0$ . Thirdly, there are different kinds of kinetic freeze out (KFO) scenarios [12–14] available in literature, it is possible that  $T_0$  can give single, double, or multiple values for the emission of different kinds of particles in various collisions. It is necessary to check the correct freeze out scenario.

The solution of all the above questions is very interesting but difficult. Particularly, the study of excitation function of  $T_0$  is required in the first issue which is already studied in our recent work [11, 15]. The second issue is analyzed and studied in [16]. It is also important to study  $T_0$  in inelastic (INEL) or non-diffractive (NSD) proton-proton (pp) collisions at RHIC and LHC energies. In case of third issue, the  $p_T$  spectra of different types of particles can be used to extract  $T_0$ , along with the accompanying results of  $\beta_T$ , which also exhibits a complex situation as  $T_0$ . Numerous methods can be used for the extraction of  $T_0$  and  $\beta_T$ . In the present work, we shall use the blast wave model with Tsallis statistics [12, 17] in order to extract  $T_0$  and  $\beta_T$  from the  $p_T$  spectra in central and peripheral gold-gold (Au-Au) and lead-lead (Pb-Pb) collisions as well as INEL or NSD pp collisions at RHIC and at LHC. The model results are compared with the experimental data measured by STAR and PHENIX collaborations. The remainder of the paper is discussed in the sections below.

## 2 The model and method

The two main processes of multi-particle production in high energy collisions are soft and hard excitation process. Soft excitation contributes in the production of most light flavor particles and is distributed in a narrow  $p_T$  range of less than 2-3 GeV/c or a little more. Generally, due to being small  $p_T$  fraction, the hard scattering process does not contribute mainly to  $T_0$  and  $\beta_T$ . In case of the narrow  $p_T$  range, we can neglect the contribution of hard scattering process. However, it is expected that the contribution fraction of hard scattering process increase with increase of collision energy. Thus,

the contribution of hard scattering process cannot be neglected in collisions at very high energy, though the soft excitation process is still the main contributor of particles production.

The description of this process has many choices of formalism which include but are not limited to the blast wave model with Tsallis statistics [12], blast wave model with Boltzmann statistics [18–20], Tsallis and related distributions with various formalisms [21–25], the (multi-) Standard distribution [26, 27], the Hagedorn thermal model [28], Erlang distribution [29–31] and the schwinger mechanism [6,32–35]. As a simple and practical application, in this work, we choose the blast-wave model with Tsallis statistics [11, 12, 19] to be more convenient due to the fact that the Tsallis and its alternative forms can be used for the fit of wider spectra, and  $T_0$  and  $\beta_T$  can easily be extracted by using the blast wave model.

According to refs. [11, 12, 19], the probability density function of  $p_T$  can be given by

$$f_1(p_T) = \frac{1}{N} \frac{dN}{dp_T} = C p_T m_T \int_{-\pi}^{\pi} d\phi \int_0^R r dr \times \left\{ 1 + \frac{q-1}{T_0} \left[ m_T \cosh(\rho) - p_T \sinh(\rho) \times \cos(\phi) \right] \right\}^{\frac{-1}{(q-1)}} \quad (1)$$

where C is the normalization constant which results in the integral of Eq. (1) to be normalized to 1,  $m_T = \sqrt{p_T^2 + m_0^2}$  is the transverse mass,  $m_0$  is the rest mass of the particle,  $\phi$  is the azimuthal angle, r is the radial coordinate, R is the maximum r, q is the entropy index,  $\rho = \tanh^{-1}[\beta(r)]$  is the boost angle,  $\beta(r) = \beta_S (r/R)^{n_0}$  is a self-similar flow profile,  $\beta_S$  is the flow velocity on the surface, and  $n_0 = 1$  is used in the original form [12]. In particular,  $\beta_T = (2/R^2) \int_0^R r \beta(r) dr = 2\beta_S / (n_0 + 2) = 2\beta_S / 3$ . The hard scattering process contributes the spectrum in wide or low+high  $p_T$  range that is described by the QCD calculus [36–38] or the Hagedorn function [28], which is an inverse power law as shown in the function below

$$f_0(p_T) = \frac{1}{N} \frac{dN}{dp_T} = A p_T \left( 1 + \frac{p_T}{p_0} \right)^{-n}, \quad (2)$$

where A is the normalization constant that normalizes the integral of Eq. (2) to unity, and  $p_0$  and n are the free parameters.

If the contributions of both the soft excitation and hard scattering processes are involved, the experimental  $p_T$  spectrum distributed in a wide range can be de-

scribed by a superposition. We have

$$f_0(p_T) = \frac{1}{N} \frac{dN}{dp_T} = k f_S(p_T) + (1 - k) f_H(p_T), \quad (3)$$

where  $k$  and  $(1 - k)$  denotes the contribution fraction of the soft excitation and hard scattering process. Naturally, the integral of Eq. (3) is normalized to 1.

According to the Hagedorn model [28], the usual step function  $\theta(x)$  can also be used in order to superimpose the contributions of soft excitation and hard scattering processes, where  $\theta(x) = 0$  if  $x < 0$  and  $\theta(x) = 1$  if  $x \geq 0$ . We have

$$\begin{aligned} f_0(p_T) &= \frac{1}{N} \frac{dN}{dp_T} \\ &= A_1 \theta(p_1 - p_T) f_S(p_T) + A_2 \theta(p_T - p_1) f_H(p_T), \end{aligned} \quad (4)$$

where  $A_1$  and  $A_2$  are the normalization constants which results in the two components to be equal to each other at  $p_T = p_1$ . The integral of Eq. (4) is normalized to 1. The contribution fraction  $k(1 - k)$  of the soft excitation (hard scattering) process is the integral of the first (second) component.

Eq. (3) and (4) are two different superpositions. Eq. (3) exhibits the contribution of soft component from 0 up to 2-3 GeV/c or a little more, which is in the low- $p_T$  region. The hard component contributes in the whole  $p_T$  range, i.e. low+high  $p_T$  region. There is overlap for the two contributions in the low- $p_T$  region due to Eq. (3). In Eq. (4), the soft component contributes from 0 to  $p_1$ , while from  $p_1$  to maximum is the contribution of hard component. There is no overlap for the two contributions due to Eq.(4).

It should be noted that in the present work, we have used Eq. (1) only, because we have used single component TBW model, but in case if the single component of the model is not enough to describe the spectra, then Eq. (3) and (4) can be used, and they are presented in order to explain the whole methodology.

To extract  $T_0$  and  $\beta_T$ , the  $p_T$  range studied in this paper is not too wide. We thus do not need to consider the contribution of hard component. Then, the second component in Eqs. (3) and (4) can be neglected. Only the first component in the two equations are necessary to consider, or in other words the two equations degrade into one, i.e. Eq. (1). In the following section, we shall only use Eq. (1) to fit the experimental data and to extract  $T_0$  and  $\beta_T$ . Before going to section 3, we would like to make it clear that there are two ways of fit. (1) Individual fit (2) Combined fit. The individual fit for each particle specie is done in our recent work. If the parameters obtained from the individual fit are similar, then we can say that the combine fit is fine. The combined

fit means that we have to use the same parameters to fit various spectra in a very narrow  $p_T$  range e.g 1-2 GeV/c for  $\pi$  and 1.5-2.6 GeV/c for  $K$ . The combined fit can be used if different  $p_T$  regions are used for different spectra.

### 3 Results and discussion

Figure 1 demonstrates the transverse momentum spectra,  $[(1/2\pi p_T) d^2N/dydp_T]$  of identified charged particles ( $\pi^-$ ,  $K^-$  and  $\bar{p}$ ) produced in (a)-(b) in the mid-rapidity range  $|y| - 0.5 < 0$  at 62.4 GeV [39] and (c)-(d) at 200 GeV [40] with Pseudo-rapidity  $|\eta| < 0.35$  in Au-Au collisions. Panel (e)-(f) corresponds to the spectra  $[(Ed^3\sigma/dp^3)]$  for  $\pi^-$ ,  $K^-$  and  $\bar{p}$  with  $|\eta| < 0.35$  produced in pp collisions at 62.4 and 200 GeV [41]. The symbols are used to represent the experimental data measured by STAR and PHENIX [39–41] Collaborations at RHIC. The solid curves are the results of our fits by using Eq.(1) and the corresponding result of their data/fit are followed in each panel. Panels (a) and (c) correspond to the central Au-Au collisions (0–10% and 0–5% centrality respectively), while panel (b) and (d) correspond to the peripheral Au-Au collisions (40–80% and 60–92% centrality respectively). The values of free parameters ( $T_0$ ,  $\beta_T$ ,  $q$ ), normalization constant ( $N_0$ ),  $\chi^2$ , and degree of freedom (dof) are listed in table 1.

Figure 2 is similar to figure 1, but it shows the transverse momentum spectra of  $\pi^-$ ,  $K^-$  and  $\bar{p}$  in panel (a)-(b) and in (c)-(d) with  $|y| < 0.5$  in Pb-Pb collisions at 2.76 [42] and 5.02 TeV [43] respectively. Panels (e) and (f) represents the transverse momentum spectra of  $(\pi^+ + \pi^-)/2$ ,  $(K^+ + K^-)/2$  and  $(p + \bar{p})/2$  with  $|y| < 1$  at 2.76 TeV [44] and  $\pi^-$ ,  $K^-$  and  $\bar{p}$  with  $|y| < 0.5$  at 5.02 TeV [43] respectively. The spectra of  $\pi^-$ ,  $K^-$  and  $\bar{p}$  for Pb-Pb central collisions at 2.76 TeV are scaled by the factor 2<sup>9</sup>. The curves are the result of our fitting by using Eq. (1), while each panel is followed by the result of its data/fit. The experimental data measured by the ALICE Collaboration [42, 43, 44] at LHC are represented by the symbols. Panels (a) and (c) corresponds to the central Pb-Pb collisions (0–5% centrality), while panel (b) and (d) corresponds to the peripheral Pb-Pb collisions (80–90% centrality).  $N_{ev}$  on the vertical axis represents the number of events. In figure 1 and 2, it can be seen that the model results describe approximately the experimental data in special  $p_T$  ranges at RHIC and LHC. It is noteworthy that in the fitting of some spectra, the  $p_T$  range is above 0.4 GeV/c due to the unavailability of  $p_T$  range less than 0.4 GeV/c.

Figure 3 shows the change in trends of the kinetic freeze out temperature ( $T_0$ ). Panel (a)-(b) show the dependence of  $T_0$  on the rest mass of the particle in cen-

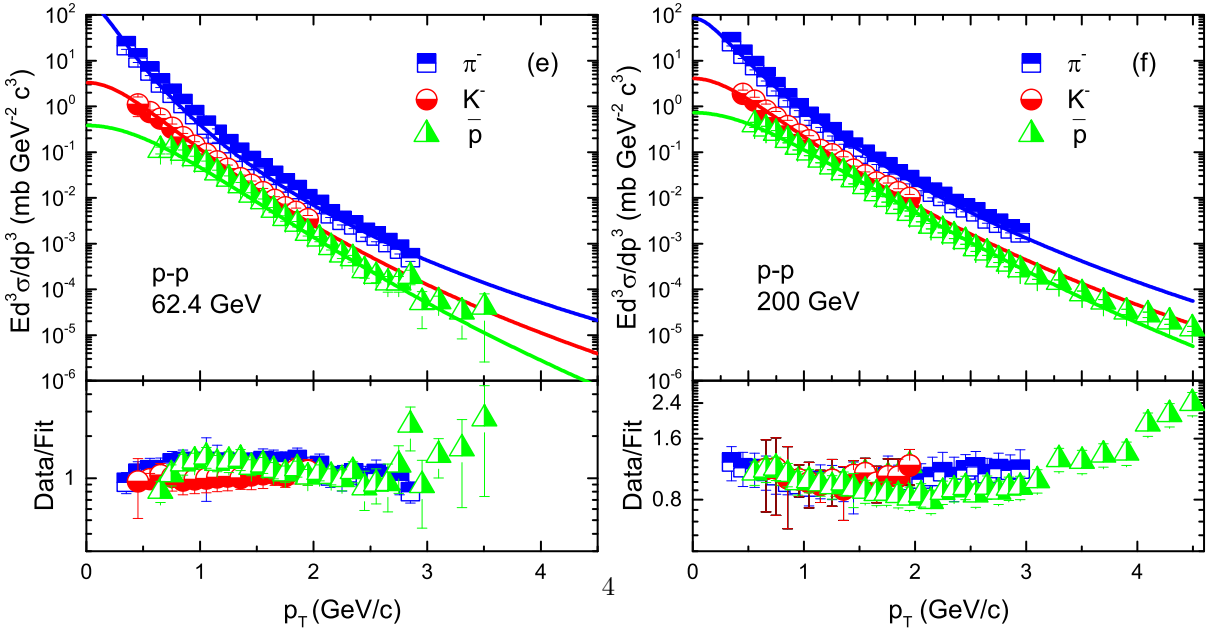
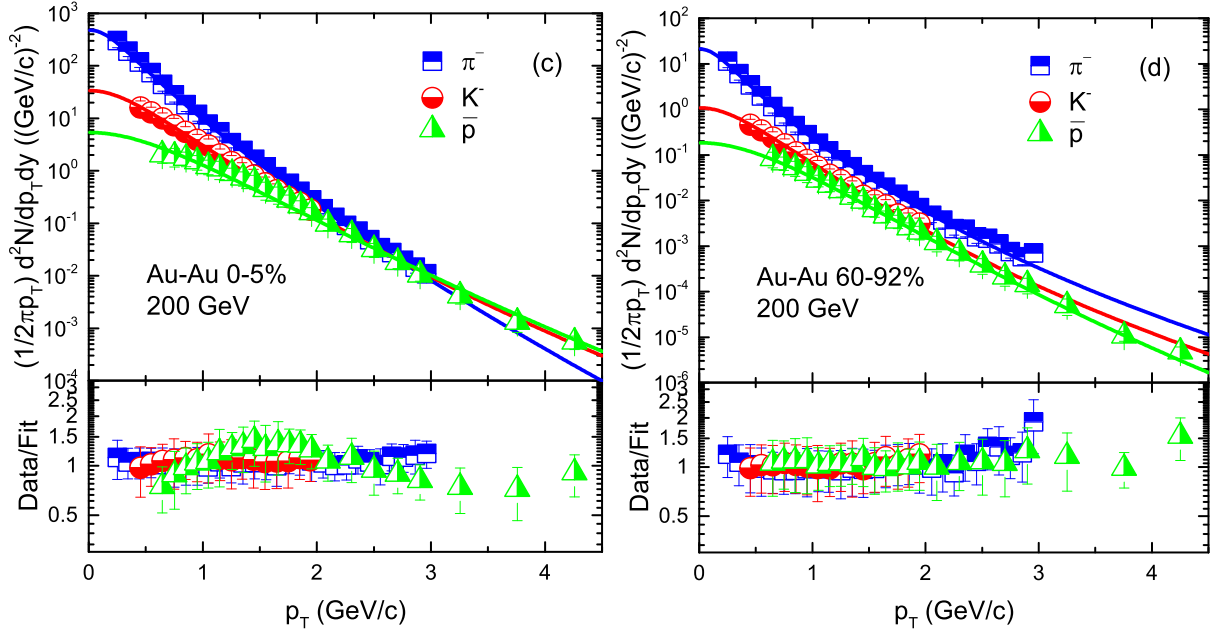
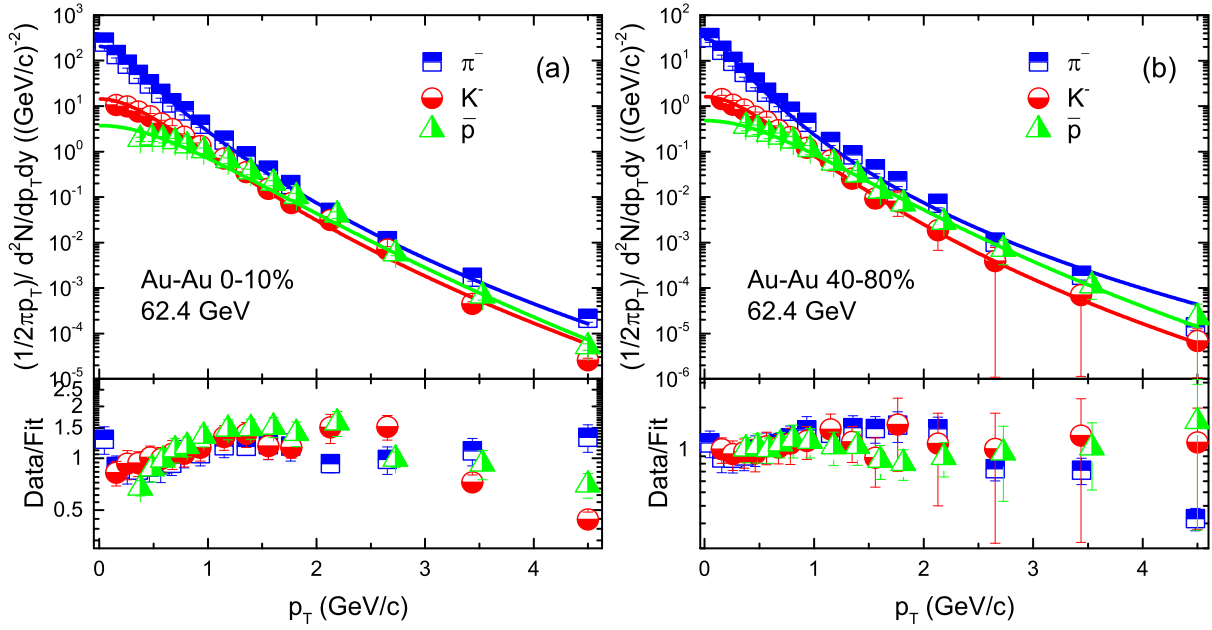


Table 1. Values of free parameters ( $T_0$  and  $\beta_T$ ), entropy index ( $q$ ), normalization constant ( $N_0$ ),  $\chi^2$ , and degree of freedom (dof) corresponding to the curves in Figs. 1–2.

| Figure                      | Centrality | Particle            | $T_0$ (GeV)       | $\beta_T$ (c)     | $q$              | $N_0$             | $\chi^2$ | dof |
|-----------------------------|------------|---------------------|-------------------|-------------------|------------------|-------------------|----------|-----|
| Fig. 1<br>Au-Au<br>62.4 GeV | 0–10%      | $\pi^-$             | $0.072 \pm 0.005$ | $0.447 \pm 0.008$ | $1.074 \pm 0.05$ | $14 \pm 2$        | 15       | 17  |
|                             |            | $K^-$               | $0.082 \pm 0.007$ | $0.415 \pm 0.009$ | $1.062 \pm 0.06$ | $2.3 \pm 0.5$     | 142      | 16  |
|                             |            | $\bar{p}$           | $0.088 \pm 0.006$ | $0.411 \pm 0.009$ | $1.050 \pm 0.05$ | $1.2 \pm 0.3$     | 68       | 14  |
|                             | 40–80%     | $\pi^-$             | $0.055 \pm 0.006$ | $0.423 \pm 0.011$ | $1.105 \pm 0.03$ | $1.5 \pm 0.35$    | 150      | 17  |
|                             |            | $K^-$               | $0.064 \pm 0.005$ | $0.390 \pm 0.012$ | $1.08 \pm 0.04$  | $2.3 \pm 0.6$     | 2        | 16  |
|                             |            | $\bar{p}$           | $0.071 \pm 0.006$ | $0.370 \pm 0.012$ | $1.07 \pm 0.03$  | $1.5 \pm 0.3$     | 3        | 14  |
| Fig. 1<br>Au-Au<br>200 GeV  | 0–20%      | $\pi^-$             | $0.094 \pm 0.006$ | $0.499 \pm 0.011$ | $1.025 \pm 0.05$ | $40 \pm 7$        | 3        | 28  |
|                             |            | $K^-$               | $0.099 \pm 0.007$ | $0.452 \pm 0.012$ | $1.05 \pm 0.04$  | $6.62 \pm 1$      | 1        | 16  |
|                             |            | $\bar{p}$           | $0.104 \pm 0.005$ | $0.439 \pm 0.009$ | $1.046 \pm 0.05$ | $2.1 \pm 0.3$     | 12       | 22  |
|                             | 60–88%     | $\pi^-$             | $0.070 \pm 0.005$ | $0.461 \pm 0.013$ | $1.07 \pm 0.05$  | $1.3 \pm 0.2$     | 5        | 28  |
|                             |            | $K^-$               | $0.077 \pm 0.005$ | $0.411 \pm 0.011$ | $1.067 \pm 0.04$ | $0.17 \pm 0.2$    | 1        | 16  |
|                             |            | $\bar{p}$           | $0.086 \pm 0.007$ | $0.390 \pm 0.008$ | $1.046 \pm 0.04$ | $0.055 \pm 0.007$ | 3        | 22  |
| Fig. 1<br>$pp$<br>62.4 GeV  | –          | $\pi^-$             | $0.040 \pm 0.005$ | $0.410 \pm 0.012$ | $1.1 \pm 0.07$   | $5.7 \pm 0.05$    | 21       | 26  |
|                             |            | $K^-$               | $0.056 \pm 0.006$ | $0.370 \pm 0.009$ | $1.078 \pm 0.06$ | $0.40 \pm 0.04$   | 1        | 16  |
|                             |            | $\bar{p}$           | $0.060 \pm 0.004$ | $0.352 \pm 0.011$ | $1.055 \pm 0.05$ | $0.09 \pm 0.05$   | 30       | 27  |
| Fig. 1<br>$pp$<br>200 GeV   | –          | $\pi^-$             | $0.065 \pm 0.007$ | $0.450 \pm 0.010$ | $1.08 \pm 0.07$  | $4.8 \pm 0.4$     | 5        | 27  |
|                             |            | $K^-$               | $0.071 \pm 0.005$ | $0.375 \pm 0.011$ | $1.078 \pm 0.05$ | $0.6 \pm 0.08$    | 4        | 16  |
|                             |            | $\bar{p}$           | $0.078 \pm 0.006$ | $0.345 \pm 0.013$ | $1.057 \pm 0.06$ | $0.2 \pm 0.03$    | 86       | 33  |
| Fig. 2<br>Pb-Pb<br>2.76 TeV | 0–5%       | $\pi^-$             | $0.108 \pm 0.007$ | $0.530 \pm 0.014$ | $1.016 \pm 0.04$ | $128.9 \pm 27$    | 89       | 40  |
|                             |            | $K^-$               | $0.111 \pm 0.005$ | $0.505 \pm 0.012$ | $1.055 \pm 0.03$ | $17.12 \pm 3$     | 30       | 36  |
|                             |            | $\bar{p}$           | $0.116 \pm 0.005$ | $0.496 \pm 0.013$ | $1.044 \pm 0.02$ | $4.9 \pm 1$       | 72       | 37  |
|                             | 70–80%     | $\pi^-$             | $0.091 \pm 0.006$ | $0.497 \pm 0.012$ | $1.053 \pm 0.03$ | $1.1 \pm 0.3$     | 209      | 40  |
|                             |            | $K^-$               | $0.094 \pm 0.005$ | $0.480 \pm 0.010$ | $1.05 \pm 0.04$  | $0.14 \pm 0.04$   | 64       | 36  |
|                             |            | $\bar{p}$           | $0.101 \pm 0.006$ | $0.470 \pm 0.009$ | $1.035 \pm 0.04$ | $0.054 \pm 0.001$ | 62       | 37  |
| Fig. 2<br>Pb-Pb<br>5.02 TeV | 0–5%       | $\pi^-$             | $0.126 \pm 0.006$ | $0.550 \pm 0.010$ | $1.01 \pm 0.05$  | $6.6 \pm 0.8$     | 756      | 35  |
|                             |            | $K^-$               | $0.128 \pm 0.005$ | $0.539 \pm 0.014$ | $1.015 \pm 0.04$ | $1.2 \pm 0.04$    | 801      | 34  |
|                             |            | $\bar{p}$           | $0.131 \pm 0.007$ | $0.528 \pm 0.010$ | $1.002 \pm 0.04$ | $3.5 \pm 0.4$     | 247      | 32  |
|                             | 60–80%     | $\pi^-$             | $0.100 \pm 0.006$ | $0.522 \pm 0.013$ | $1.05 \pm 0.06$  | $4.2 \pm 0.4$     | 435      | 35  |
|                             |            | $K^-$               | $0.113 \pm 0.005$ | $0.516 \pm 0.009$ | $1.04 \pm 0.05$  | $0.90 \pm 0.04$   | 73       | 34  |
|                             |            | $\bar{p}$           | $0.121 \pm 0.007$ | $0.502 \pm 0.012$ | $1.015 \pm 0.04$ | $6.5 \pm 0.3$     | 261      | 32  |
| Fig. 2<br>$pp$<br>2.76 TeV  | –          | $(\pi^+ + \pi^-)/2$ | $0.087 \pm 0.006$ | $0.486 \pm 0.008$ | $1.046 \pm 0.03$ | $0.35 \pm 0.06$   | 385      | 22  |
|                             |            | $(K^+ + K^-)/2$     | $0.091 \pm 0.007$ | $0.468 \pm 0.012$ | $1.04 \pm 0.04$  | $0.048 \pm 0.005$ | 8        | 17  |
|                             |            | $(p + \bar{p})/2$   | $0.097 \pm 0.005$ | $0.448 \pm 0.011$ | $1.03 \pm 0.04$  | $0.02 \pm 0.007$  | 13       | 27  |
| Fig. 2<br>$pp$<br>5.02 TeV  | –          | $\pi^-$             | $0.094 \pm 0.006$ | $0.513 \pm 0.013$ | $1.13 \pm 0.05$  | $1.6 \pm 0.3$     | 235      | 35  |
|                             |            | $K^-$               | $0.098 \pm 0.007$ | $0.491 \pm 0.012$ | $1.12 \pm 0.07$  | $0.34 \pm 0.06$   | 904      | 33  |
|                             |            | $\bar{p}$           | $0.103 \pm 0.005$ | $0.481 \pm 0.011$ | $1.096 \pm 0.05$ | $0.16 \pm 0.04$   | 412      | 31  |

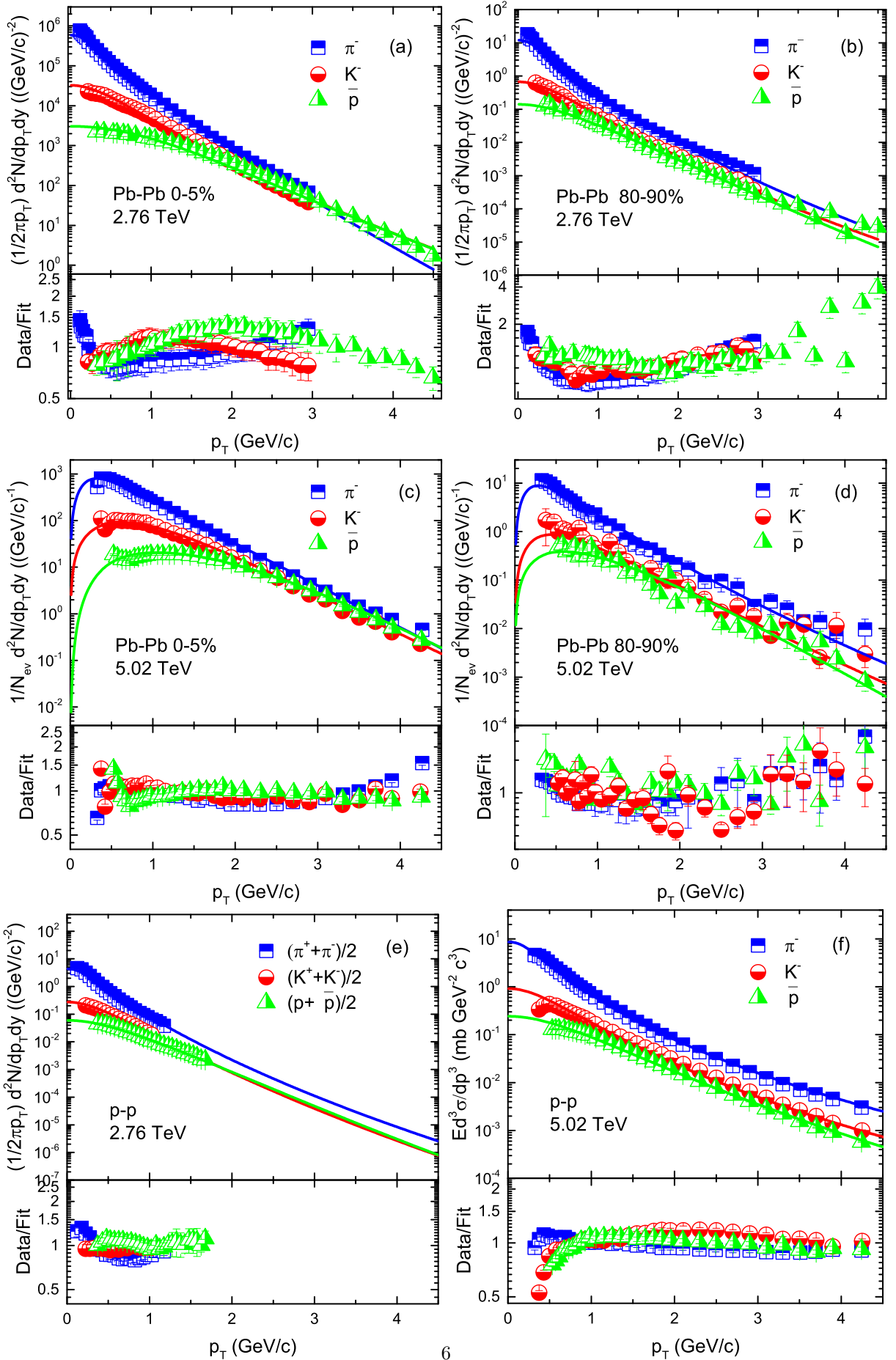


Fig. 2. is similar to fig. 1, but shows the spectra of the particles in Pb-Pb collision from panel (a)-(d), as well

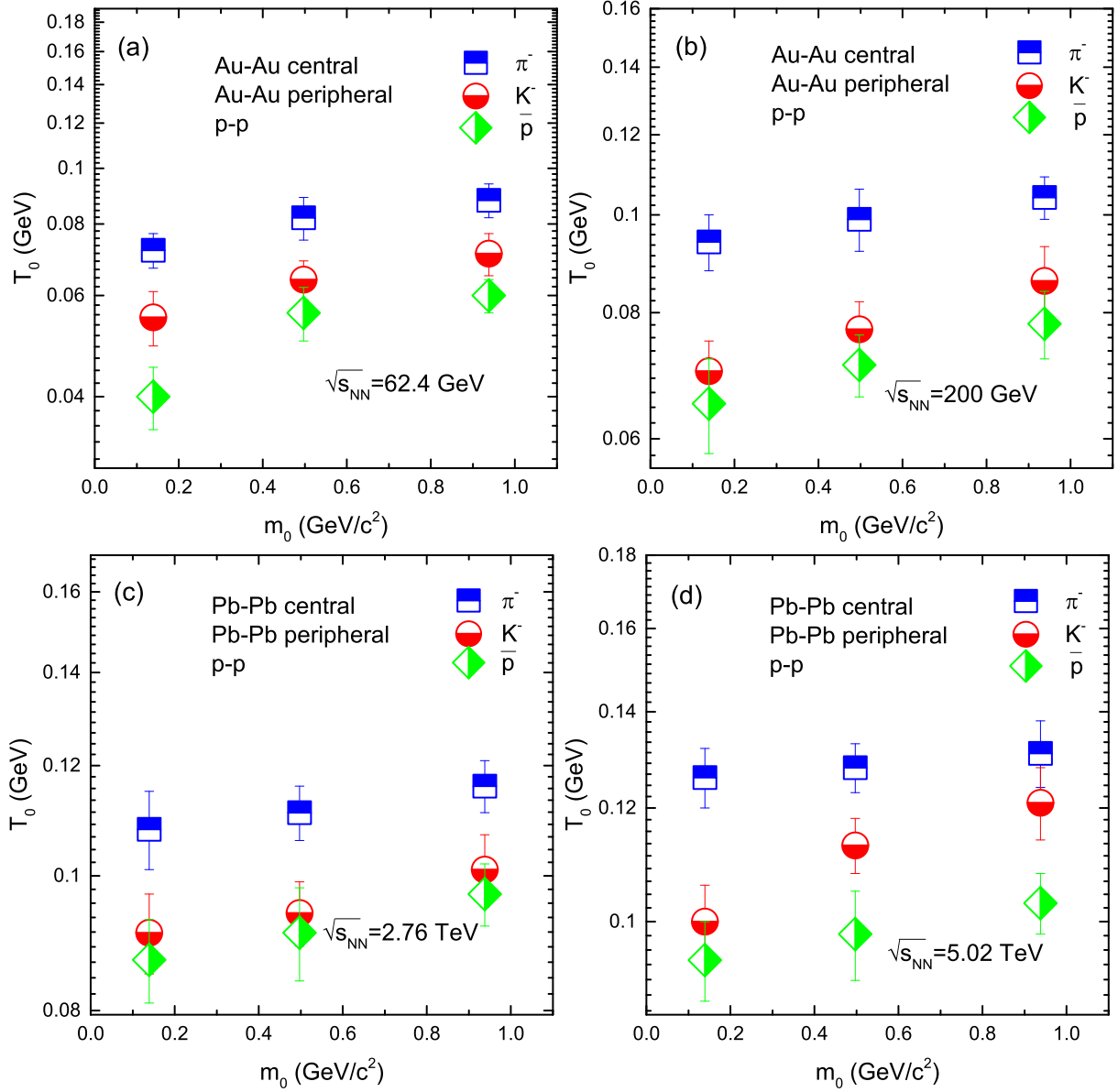


Fig. 3. (a)-(b): Dependence of  $T_0$  on  $m_0$  in Au-Au central and peripheral as well as in pp collisions at 62.4 GeV and 200 GeV respectively. (c)-(d)dependence  $T_0$  on  $m_0$  in Pb-Pb central and peripheral as well as in pp collisions at 2.76 TeV and 5.02 TeV respectively.

tral and peripheral Au-Au as well as in pp collisions at 62.4 GeV and 200 GeV respectively, While panel (c)-(d) show the dependence of  $T_0$  on the rest mass of the particle in central and peripheral Pb-Pb as well in pp collisions at 2.76 TeV and 5.02 TeV respectively. Different symbols represent the values of parameter ( $T_0$ ) for different particles in different collisions. One can see that the values of  $T_0$  for heavier particles are larger than that for the lighter particles, which show the early freeze out of the heavier particles compared to the lighter particles. The different freeze out for different particles reveal the mass differential freeze out (multiple freeze out) scenario. Furthermore,  $T_0$  in the central nucleus-nucleus (AA) collisions is larger than in peripheral collisions due to the reason that central collision involves more participant nucleons in interaction, so the collision is more violent and the system gets higher degree of excitation, while the peripheral collision involves less participants and attains low degree of excitation in the interaction which results in smaller  $T_0$ . Larger  $T_0$  in central collisions indicates quicker approach of equilibrium of the system.  $T_0$  is also analyzed in pp collisions at RHIC and LHC energies. It is observed that  $T_0$  in peripheral AA collisions is slightly larger than in pp collisions at the same center of mass energy due to the involvement of more participant nucleons in former interaction as compared to the later, or it is approximately equal in both these collisions at the same center of mass energy due to a not violent interaction and the later statement indicates almost the same thermodynamic nature of the parameters in the corresponding collisions of the same center of mass energy (per nucleon pair). It is also observed that  $T_0$  in Pb-Pb collisions is larger than in Au-Au collisions, and in AA collisions, it is larger than in pp collisions, which may indicate its dependence on the size of interacting system. The present work also shows the energy dependence of in AA and pp collisions.  $T_0$  dependence on energy and on the size of the interacting system (in AA or pp collisions) is a huge project which requires a lot of data, therefore we will keep this project in future consideration.

The transverse flow velocity ( $\beta_T$ ) dependence on  $m_0$  and centrality is shown in figure 4. It can be obviously seen that  $\beta_T$  in Au-Au and Pb-Pb central collisions is larger than in peripheral collisions, due to the involvement of large number of participants in the interaction which results in more energy deposition in the central collisions and the fireball expands more rapidly. The heavier particles are observed to have smaller values of  $\beta_T$  as compared to the light particles. Furthermore,  $\beta_T$  in AA peripheral collisions is slightly larger than or almost equivalent to pp collisions at the same center of mass energy (per nucleon pair), and the collisions in

both the peripheral AA and pp interaction are not violent due to the involvement of few nucleons in interaction and the fireball does not expand quickly. Like  $T_0$  in figure 3,  $\beta_T$  in figure 4 is increasing with energy and also with the size of the interacting system.

Figure 5 represents the dependence of the entropy index ( $q$ ) on  $m_0$  and centrality. Different symbols and different colors represent different collisions and different particles. From fig. 5(a)-(d), one can see that in most cases,  $q$  is larger for the lighter particles compared to heavier particles. e.g pion is larger than the rest of two in most cases which shows that the production of pion is more polygenetic than the others. Additionally,  $q$  is larger in the peripheral and pp collisions compared to the central collisions which indicates that the central nucleus-nucleus collisions has a quick approach to equilibrium state as compared to the peripheral nucleus-nucleus and pp collisions.

We would also like to point out that the values of normalization constant ( $N_0$ ) in table 1 are mass dependent, and  $N_0$  decrease with increasing the rest mass of the particle.

Before going to the conclusions, we would like to give more explanation of  $p_T$  spectra and the parameters extracted from it. The structure of  $p_T$  spectra of the particles in high energy collisions is very complex. Except the soft and hard  $p_T$  regions, there also exists the very soft and very hard  $p_T$  regions. The detail of the four  $p_T$  regions can be found briefly in [45]. The  $p_T$  region of  $p_T < 0.2-0.3$  is considered to be the very soft region. The very soft  $p_T$  region contributes to the production of resonance which changes the slopes of the  $p_T$  spectra and affects the values of free parameters. For-example, the large contribution of resonance tends to reduce  $T_0$  and increase  $\beta_T$  and this idea is giving strength to our current conclusion of the multiple kinetic freeze out scenario. Among the considered particles, pion is largely influenced by the resonance [46, 47] and proton is more stable [42]. However, at higher  $p_T$ , the hagedorn function contributes and it will not effect  $T_0$  and  $\beta_T$ .

The situation of  $T_0$  and/or  $\beta_T$  are very complex on the basis of their dependence on energy and/or centrality. Different models are analyzed in [48] which shows different results of  $T_0$  and  $\beta_T$ . In addition, in [49], from RHIC to LHC,  $T_0$  increase  $\sim 9\%$  and  $\beta_T$  increase  $\sim 65\%$ . However, from RHIC to LHC,  $T_0$  decrease  $\sim 5\%$  while an increase  $\sim 20\%$  in  $\beta_T$  from 39 to 200 GeV can be seen in [50, 51]. In [52, 53] there is no obvious change observed in  $T_0$  from RHIC to LHC, however  $\beta_T$  shows an increase of  $\sim 10\%$ . Our recent results are similar to the above mentioned works although the concrete values are not the same, especially, at least one can observe the increasing excitation function of  $\beta_T$  with the increasing

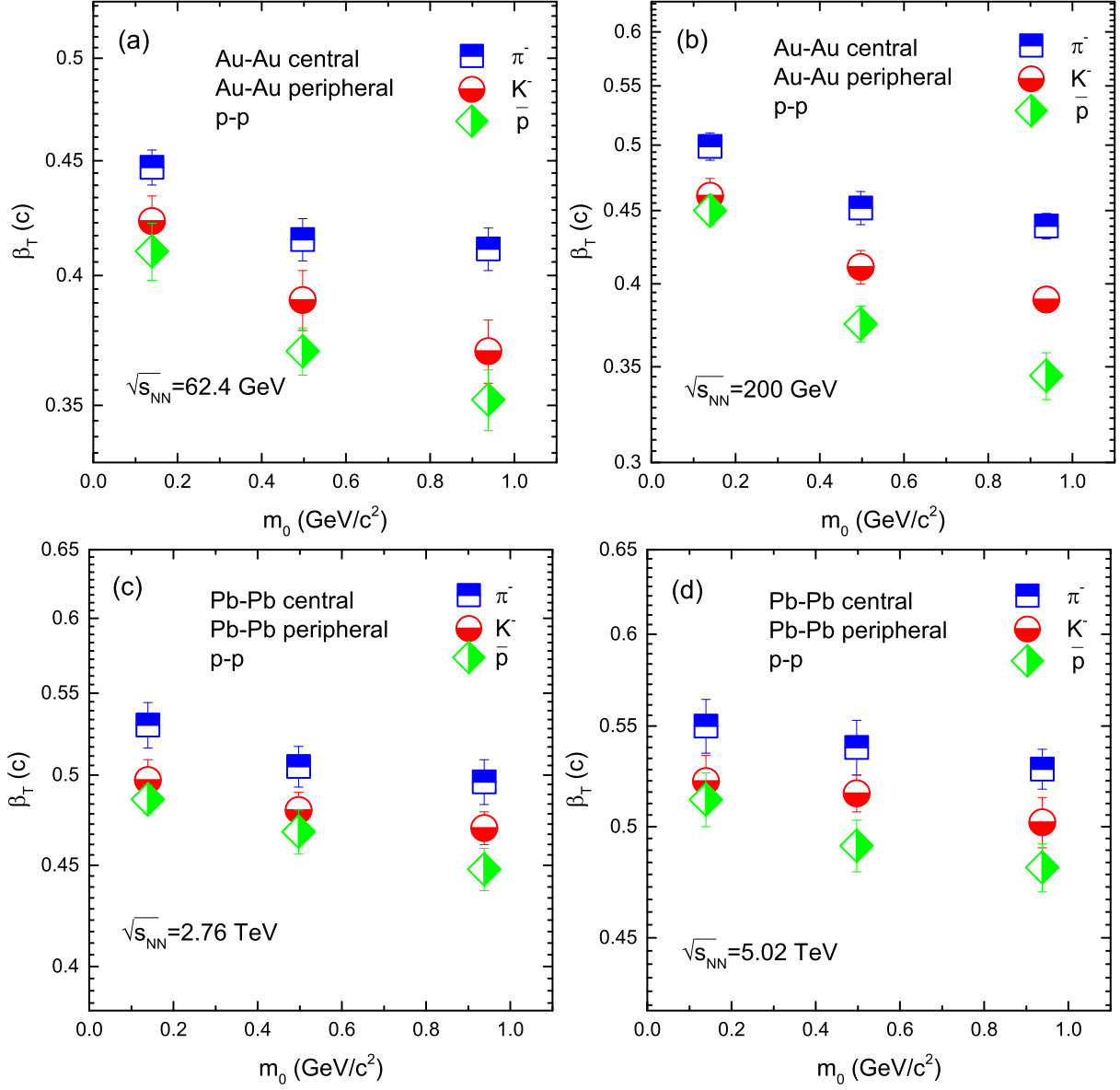


Fig. 4. (a)-(b): Dependence of  $\beta_T$  on  $m_0$  in Au-Au central and peripheral as well as in pp collisions at 62.4 GeV and 200 GeV respectively. (c)-(d) dependence  $\beta_T$  on  $m_0$  in Pb-Pb central and peripheral as well as in pp collisions at 2.76 TeV and 5.02 TeV respectively.

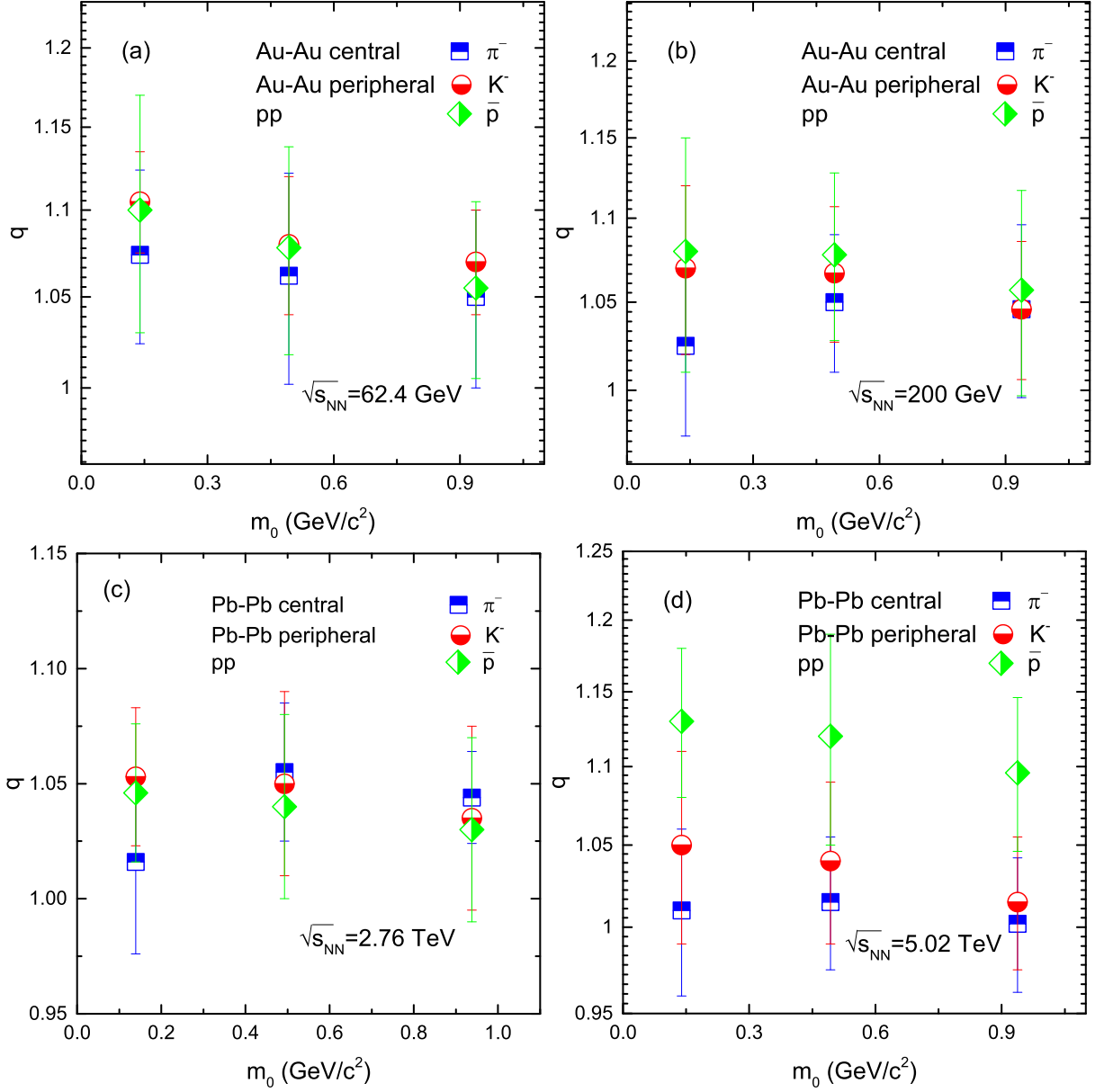


Fig. 5. (a)-(b): Dependence of  $q$  on  $m_0$  and centrality in Au-Au central and peripheral as well as in pp collisions at 62.4 GeV and 200 GeV respectively. (c)-(d) dependence  $q$  on  $m_0$  and centrality in Pb-Pb central and peripheral as well as in pp collisions at 2.76 TeV and 5.02 TeV respectively.

energy. In addition,  $T_0$  and  $\beta_T$  show different trend from central to peripheral collisions in different literatures. In [10, 54, 55],  $T_0$  is increasing from central to peripheral collisions. Our present work is inconsistent with [10, 54, 55], but consistent with [15, 45, 56] which gives larger  $T_0$  in central collisions. Both the above mentioned school of thoughts about the trend  $T_0$  has their own explanations. The present work explains the higher degree of excitation of the interacting system in the central collisions due to large number of participants involved in the interaction and more energy is stored in the system. On the other hand, the larger  $T_0$  in the peripheral collisions explain the longer lifetime of the fireball in the central collisions. It is noteworthy that the present work results for  $T_0$  are not consistent with [10, 54, 55] due to different methods and model with different conditions and limitations. Even by using the same model with different method and different conditions and limitations, we can get the different results, e:g in our recent work [15] and in [10, 54, 55] the blast wave model with boltzmann Gibbs statistics with different conditions and limitations is used and the result is different.

It should be noted that Blast wave model with boltzmann Gibbs statistics (BGBW) has been extensively used for the description of the produced system at thermal/kinetic freezeout temperature. It is assumed by the BGBW model that the produced system has reached to thermal equilibrium so that a Boltzmann distribution with a radial profile can be used for the description of  $p_T$  spectra [18]. Nonetheless, the very limited low  $p_T$  spectra can be described by the equilibrium distribution and is sensitive to the choice of specific  $p_T$  spectra (cover narrow  $p_T$  range). Later, the Tsallis statistics was introduced to describe the particle production for an extended  $p_T$  range (up to 5 GeV/c) in high energy collisions [57, 58, 59, 60, 61, 62]. The advantage of Tsallis statistics is that it introduces a new parameter "q" that describes the degree of non-equilibrium in the system, which is helpful in pp collisions [19] and AA peripheral collisions specially. The parameter q=1 in BGBW, while in TBW model q<1.25, which affects the  $p_T$  range but it is not responsible to change the trend of the results.

It should be noted that there exists an entanglement in the extraction of  $T_0$  and  $\beta_T$ . In deed, if for central collisions, one use a smaller  $T_0$  and a larger  $\beta_T$ , a decreasing trend for  $T_0$  from peripheral to central collisions can be obtained. At the same time, a negative correlation between  $T_0$  and  $\beta_T$  will also be obtained. Thus, this situation is in agreement with some references [10, 42, 55, 64, 65], but if for central collisions, one even uses an almost unchanging or slightly larger  $T_0$  and a properly larger  $\beta_T$ , an almost invariant or slightly increasing

trend for  $T_0$  from peripheral to central collisions can be obtained [7, 15, 56, 63]. In order to show the flexibility in the extraction of  $T_0$  and  $\beta_T$ , this work has reported a decreasing trend for  $T_0$  from central to peripheral collisions, and a positive correlation between  $T_0$  and  $\beta_T$ .

In addition, we would point out that the present work is in agreement as well as in disagreement with some works. This is due to different models or methods as discussed before. In the present work we have used the least square method with different conditions. We have used slightly lager  $T_0$  and  $\beta_T$  in central collisions and obtained larger  $T_0$  in central collisions as compared to peripheral collisions, and the same conditions with the same method is used in [15, 45, 56]. Furthermore, the present work used  $n_0=1$  which is in close resemblance with hydrodynamic profile as mentioned in [66].  $n_0=2$  is also a close approximation to the hydrodynamic profile according to reference [18].  $n_0=1$  or 2 does not effect the curve as well as the free parameters. If one consider the quick decay of  $\beta_r$  from the surface to the center of emission source, one should use  $n_0=2$ , but if the  $\beta_r$  decay from the surface to the center emission source is not quick, then  $n_0=1$  will be used. Anyways, we did not regard  $n_0$  as a free parameter which is too inconsistent and arguable in our opinion and it can have an effect on curve as well as on the free parameters. According to [67], apart from the fact that  $n_0$  is mutable (from  $0.0\pm 10.1$  to  $4.3\pm 1.7$ ), but the  $p_T$  coverage is also narrow and particle dependent ( $p_T\approx 0.20-0.70$  GeV/c,  $0.25-0.75$  GeV/c and  $0.35-1.15$  GeV/c for  $\pi^+$ ,  $K^+$  and p respectively), that uses a single kinetic freeze out scenario and give different result of  $T_0$  and  $\beta_T$  from this work. If  $n_0$  is regarded as a free parameter and the particle dependent and narrow  $p_T$  coverage is used, similar result with [67] can be obtained.

In fact, many uncertainties arise from the fit function choice as well as from the flow profile and also from the well-known ambiguity in the fit results. It is always possible to trade  $T_0$  against  $\beta_T$  in a single  $p_T$  spectrum. That is for a given  $p_T$  spectrum, there is a negative correlation among  $T_0$  and  $\beta_T$ . It is possible that we may obtain a positive or negative correlation if we use a suitable  $T_0$  and  $\beta_T$  for a set of  $p_T$  spectra. In fact, there is an influence if a changeable  $p_T$  and /or  $n_0$  choice on the extraction of the two parameters are used. In our opinion, if we use a fixed flow profile ( $n_0$ ) and wide and fixed  $p_T$  coverage for various particles, the uncertainties can be reduced.

## 4 Conclusions

The main observations and conclusions are summa-

rized here.

(a) The transverse momentum spectra of the identified charged particles  $[(\pi^-, K^- \text{ and } \bar{p}) \text{ or } (\pi^+ + \pi^-, K^+ + K^- \text{ and } p + \bar{p})]$  produced in central and peripheral Au-Au and Pb-Pb collisions as well as in pp collisions at RHIC and LHC energy have been analyzed by TBW model. The model results are in agreement with the experimental data in the special  $p_T$  range measured by STAR, PHENIX, and ALICE collaborations.

(b) Kinetic freeze out temperature and transverse flow velocity are extracted from the transverse momentum spectra fitting. Both  $T_0$  and  $\beta_T$  are observed to be larger in central collisions than the peripheral collisions, and the results for  $T_0$  and  $\beta_T$  at LHC are observed to be larger than that at RHIC, which shows their dependence on the collision energy.

(c)  $T_0$  and  $\beta_T$  are mass dependent,  $T_0$  increase with increase of  $m_0$  which reveals the multiple kinetic freeze out scenario, however  $\beta_T$  decrease with  $m_0$ .

(d) The kinetic freeze out temperature and transverse flow velocity in peripheral Au-Au collisions and pp collisions at 62.4 and 200 GeV as well as in peripheral Pb-Pb collisions and pp collisions at 2.76 and 5.02 TeV are similar and have similar trend which exhibits the similar thermodynamic nature of the parameters in peripheral AA and pp collisions at the same center of mass energy (per nucleon pair).

### Acknowledgments

The authors would like to thank support from the National Natural Science Foundation of China (Grant Nos. 11875052, 11575190, and 11135011).

### References

- [1] D. D. Ivanenko, D. F. Kurdgelaidze. *Ast. Phys.* 1, 251 (1965).
- [2] J. F. Xu et. al, *Phy. Rev. D* 92, 025025 (2015).
- [3] T. D. Lee, G. C. Wick. *Phys. Rev. D* 9, 2291 (1974) .
- [4] D. H. Rischke. *Prog. Part. Nucl. Phys.* 52, 197 (2004).
- [5] I. Arsene et al. (BRAMHS Collaboration). *Nucl. Phys. A* 757, 1 (2005).
- [6] A. Puglisi, A. Sarracino, A. Vulpiani, *Phys. Rep.* 709, 1 (2017).
- [7] M. Waqas, Fu. Hu. Liu, *Eur. Phys. J. Plus* 135, 147 (2020).
- [8] A. Andronic, P. Braun-Munzinger and J. Stachel, *Nucl. Phys. A* 772, 167 (2006).
- [9] J. Cleymans, H Oeschler, K Redlich and S Wheatson, *Phys. Rev. C*, 73, 034905 (2006).
- [10] Lokesh Kumar et al. (STAR Collaboration), *Nucl. Phys. A* 931, 1114 (2014).
- [11] Muhammad Waqas, Fu-Hu Liu, Rui-Qin Wang, Irfan Siddique, *Eur. Phys. J. A*, 56, 188 (2020).
- [12] Z. B. Tang, Y. C. Xu, L. J. Ruan, G. van Buren, F. Q. Wang, Z. B. Xu, *Phys. Rev. C*, 79, 051901 (2009).
- [13] S. Chatterjee, B. Mohanty, R. Singh, *Phys. Rev. C*, 89, 034908 (2014).
- [14] S. Chatterjee, B. Mohanty, Bedangadas, R. Singh, *Phys. Rev. C*, 92, 024917 (2015).
- [15] Muhammad Waqas, Bao-Chun Li, *Adv. High Energy Phys* 2020, 1787183 (2020).
- [16] H-L Lao, Fu-Hu Liu, B-C Li and M. Y. Duan, *Roy A. Lacey, Nucl. Sci. Tech*, 29, 164 (2018).
- [17] Li-Li Li, Fu-Hu Liu, *MDPI Physics*, 2, 277–308 (2020).
- [18] E. Schnedermann, J. Sollfrank and U. W. Heinz, *Phys. Rev. C*, 48, 2462 (1993).
- [19] K. Jiang, Y.Y. Zhu, W.T. Liu, H.F. Chen, C. Li, L.J. Ruan, Z.B. Tang, Z.B. Xu, *Phys. Rev. C*, 91,024910 (2015).
- [20] STAR Collaboration (B.I. Abelev et al.), *Phys. Rev. C* 79, 034909 (2009).
- [21] Hai-Ling Lao, and Hua-Rong Wei, Fu-Hu Liu, Roy A. Lacey, *Eur. Phys. J. A*, 52, 203 (2016).
- [22] J. Cleymans, D. Worku, *Eur. Phys. J. A*, 48, 160 (2012).
- [23] J.M. Conroy, H.G. Miller, *Phys. Rev. D* 78, 054010 (2008).
- [24] A.M. Teweldeberhan, A.R. Plastino, H.G. Miller, *Phys. Lett. A* 343, 71 (2004).
- [25] J.M. Conroy, H.G. Miller, A.R. Plastino, *Phys. Lett. A* 374, 4581 (2010).
- [26] Li-Li Li, Fu-Hu Liu, Muhammad Waqas, Rasha Al-Yusufi, Altaf Mujear, *Adv. High Energy Phys*, 2020, 5356705 (2020).
- [27] Muhammad Waqas, Fu-Hu Liu, Zafar Wazir, *Adv. High Energy Phys*, 2020, 8198126 (2020).
- [28] R. Hagedorn, *Riv. Nuovo Cimento* 6(10), 1 (1983).
- [29] Li-Na Gao, Fu-Hu Liu, Qin Ya , Tian Tian, Bao-Chun Li, *Eur. Phys. J. A*, 520, 94 (2014).
- [30] Li-Na Gao, Fu-Hu Liu, Roy A Lacey, *Eur. Phys. J. A*, 52, 137 (2016).
- [31] Wen-Jie Xie, *Chin. Phys. C*, 35, 1111–1119 (2011).
- [32] R.-C. Wang and C.-Y. Wong, *Phys. Rev. D* 38, 348 (1988).
- [33] S. Tahery and X. Chen, arXiv: 2007.01559 [hep-th].
- [34] H. Taya, arXiv: 2003.12061 [hep-ph].
- [35] H. Taya, arXiv: 2003.08948 [hep-ph].
- [36] N. A. Abdulov, A. V. Lipatov and M. A. Malyshev, *Phys. Atom. Nucl.* 82, 1602–1606 (2020).
- [37] M. Mieskolainen, [arXiv: 1910.06279 [hep-ph]].
- [38] J. Mashford, [arXiv: 1809.04457 [physics.gen-ph]].
- [39] M. Shao [for the STAR Collaboration], *J. Phys. G* 31,S85 (2005).
- [40] S. S. Adler *et al.* [PHENIX Collaboration], *Phys. Rev. C*. 69, 034909 (2004).
- [41] A. Adare *et al.* [PHENIX Collaboration], *Phys. Rev. C* 83, 064903 (2011).
- [42] B. Abelev *et al.* [ALICE Collaboration], *Phys. Rev. C* 88, 044910 (2013).

- [43] Y. C. Morales, N. Hussain, N. Jacazio, A. Ortiz I Ravasenga, O. Vazquez5 and G Volpe, [ALICE Collaboration], Preprint ALICE-ANA-2016-XXX (july 2017).
- [44] P. K. Khandai, P. Sett, P. Shukla and V. Singh, Int. J. Mod. Phys. A 28, 1350066 (2013), [arXiv:1304.6224 [hep-ph]]. doi:10.1142/S0217751X13500668.
- [45] M. Waqas and F. H. Liu, doi: 10.1007/s12648-021-02058-5; [arXiv:1806.05863 [hep-ph]].
- [46] N. Yu and X. Luo, Eur. Phys. J. A 55, 26 (2019). doi:10.1140/epja/i2019-12691-8 [arXiv:1810.09101 [hep-ph]].
- [47] J. Cleymans, B. Kampfer and S. Wheaton, Phys. Rev. C 65, 027901 (2002). doi:10.1103/PhysRevC.65.027901 [arXiv:nucl-th/0110035 [nucl-th]].
- [48] H.-L. Lao, ; F.-H. Liu, ; B.-C. Li, ; M.-Y. Duan, Nucl. Sci. Tech. 29, 82 (2018).
- [49] Zhang, S.; Ma, Y.G.; Chen, J.H.; Zhong, C. Adv. High Energy Phys. 2015, 460590 (2015).
- [50] Das, S. In EPJ Web of Conferences; EDP Sciences: Jules, France; Volume 90, 08007 (2015).
- [51] Das, S.; Nucl. Phys. A 904 C905, 891c C894c (2013).
- [52] Andronic, A. Int. J. Mod. Phys. A 29, 1430047 (2014).
- [53] Abelev, B.; ALICE Collaboration. Phys. Rev. Lett. 109, 252301 (2012).
- [54] S. Acharya *et al.* [ALICE], Phys. Rev. C 101, 044907 (2020). doi:10.1103/PhysRevC.101.044907 [arXiv:1910.07678 [nucl-ex]].
- [55] L. Adamczyk *et al.* [STAR], Phys. Rev. C 96, 044904 (2017) doi:10.1103/PhysRevC.96.044904 [arXiv:1701.07065 [nucl-ex]].
- [56] Q. Wang and F. H. Liu, Int. J. Theor. Phys. 58, no.12, 4119-4138 (2019). doi:10.1007/s10773-019-04278-2 [arXiv:1909.02390 [hep-ph]].
- [57] B. De, S. Bhattacharyya, G. Sau and S. K. Biswas, Int. J. Mod. Phys. E 16 1687-1700 (2007) doi:10.1142/S0218301307006976
- [58] G. Wilk and Z. Wlodarczyk, Eur. Phys. J. A 40 299 (2009).
- [59] W. M. Alberico, A. Lavagno and P. Quarati, Eur. Phys. J. C 12 499-506 (2000) doi:10.1007/s100529900220 [arXiv:nucl-th/9902070 [nucl-th]].
- [60] T. Osada and G. Wilk, Phys. Rev. C 77 044903 (2008) Erratum: [Phys. Rev. C 78, 069903 (2008)]
- [61] T. S. Biro and B. Muller, Phys. Lett. B 578 78-84 (2004) doi:10.1016/j.physletb.2003.10.052 [arXiv:hep-ph/0309052 [hep-ph]].
- [62] T. Bhattacharyya, J. Cleymans, A. Khuntia, P. Parreek and R. Sahoo, Particle Spectra at LHC in the Limit of Small ( $q - 1$ ),” Eur. Phys. J. A 52 30 (2016) doi:10.1140/epja/i2016-16030-5 [arXiv:1507.08434 [hep-ph]].
- [63] M. Waqas, G. X. Peng and F. H. Liu, J. Phys. G 48, 075108 (2021). doi:10.1088/1361-6471 [arXiv:2101.07971 [hep-ph]].
- [64] A. Khuntia, H. Sharma, S. K. Tiwari, R. Sahoo, and J. Cleymans, Eur. Phys. J. A 55, 3 (2019), doi:10.1140/epja/i2019-12669-6.
- [65] M. Waqas and G. X. Peng, Adv. High Energy Phys. 2021 (2021), 6674470, doi:10.1155/2021/6674470, [arXiv:2103.07852 [hep-ph]].
- [66] P. F. Kolb and U. Heinz, ”Hydrodynamic description of ultrarelativistic heavy ion collisions,” in Quark-Gluon Plasma 3, Edited by R. C Hwa and X.-N Wang (World Scientific Singapore) (2004), doi:10.1142/5029.
- [67] B. I. Abelev et al. (STAR Collaboration), Phys. Rev. C 81, 024911 (2010), doi:10.1103/PhysRevC.81.0214911.